

A simple retrieval method for land surface temperature and fraction of water surface determination from satellite microwave brightness temperatures in sub-arctic areas

M. Fily^{a,*}, A. Royer^b, K. Goïta^b, C. Prigent^c

^aLaboratoire de Glaciologie et Géophysique de l'Environnement, CNRS/Université Joseph Fourier, Domaine Universitaire, BP96, 38402 Saint Martin d'Hères Cedex, France

^bCARTEL, Université de Sherbrooke, 2500 Boul. Université, Sherbrooke, Quebec, Canada J1K 2R1

^cObservatoire de Paris, 61 Av. de l'Observatoire, 75014, Paris, France

Received 20 June 2002; received in revised form 15 October 2002; accepted 15 December 2002

Abstract

A strong linear relationship is found between Special Sensor Microwave/Imager (SSM/I) microwave (19 and 37 GHz) surface emissivities at horizontal and vertical polarizations over snow- and ice-free land surfaces. This allows retrieving the land surface emissivity and temperature from satellite microwave brightness temperatures after atmospheric corrections. Over the Canadian sub-arctic continental area, we show that the main factor modifying the emissivity is the fraction of water surface (FWS) within a pixel. Accordingly, a map of the fraction of water surface across the Canadian landmass is derived, given a correspondence within 6% as compared to the 1 km² Canadian National Topographic Database of water-covered areas. The microwave-derived surface temperatures are compared to synchronous in situ air and ground surface temperatures and also with independent satellite IR measurements over areas without snow or ice. Root mean square differences range between 2° and 3.5°, with mean bias error of the order of 1–3°. Better results are always obtained with the 37 GHz channel rather than with the 19 GHz channel. Over dense vegetation, the microwave-derived surface temperature is closer to the air temperature (at surface level) than to the ground temperature. The proposed simple retrieval algorithm, not sensitive to cloud cover, appears very useful for monitoring summer interannual or seasonal trends of the fraction of surface water, as well as the daily land surface temperature variation, which are very important parameters in environmental change analysis.

© 2003 Elsevier Science Inc. All rights reserved.

Keywords: Remote sensing; Temperature; Surface water; Microwave; Canada

1. Introduction

State-of-the-art scenarios of future climate evolution predict that climate change will be particularly strong in the high latitudes and that permafrost zones, representing 25% of the continental surface in the northern hemisphere, could be among the most strongly affected regions (CLIC, 2001; Serreze et al., 2000). Historical temperature trends show a warming of nearly 2 °C during the last century in the western Canadian Arctic and this warming is expected to have significant impact on the stability of permafrost (Smith

& Burgess, 1998). Warming of permafrost could also have significant impacts on the carbon cycle as it could alter carbon sources and sinks in organic terrain, and it could result in the release of additional carbon, which is currently stored as methane in gas hydrates. Climate warming could moreover generate important hydrological repercussions. Changes in seasonally frozen ground and permafrost, and in storage of water in snow which is the major source of freshwater for main hydrological systems and reservoirs could induce significant feedback processes of surface energy and moisture exchange between the cryosphere, the hydrosphere, and the atmosphere (Smith, Burgess, & Heginbottom, 2001). Further knowledge of these issues is essential towards understanding recent climate change and future trends. In situ measurements for permafrost state evolution as well as soil moisture variation are scarce

* Corresponding author. Tel.: +33-4-76-82-42-35; fax: +33-4-76-82-42-01.

E-mail address: fily@lgge.obs.ujf-grenoble.fr (M. Fily).

(Burgess, Smith, Brown, & Romanovsky, 2001). Only remote sensing allows measurements at the continental scale and it is crucial to develop new methods to invert surface parameters from satellite measurements.

Passive microwave measurements are independent of solar illumination and information from the surface can be acquired even through clouds as opposed to optical sensors. Accordingly, they are useful tools for sub-arctic areas where cloud cover is frequent and solar illumination is quite variable throughout the year. Almost daily data are available from microwave radiometers compared to optical sensors where, most of the time, only weekly or decadal time series products are available. Their coarse spatial resolution is not a major problem for large scale studies and 20-year time series are now available which are of great interest for recent climate change studies (Cavalieri, Gloersen, Parkinson, Comiso, & Zwally, 1997; Chang, Foster, & Hall, 1987; Grody & Basist, 1996; Torinesi, Fily, & Genthon, in press).

Passive microwave data have already been used for land surface temperature determination (Aires, Prigent, Rossow, & Rothstein, 2001; Basist, Grody, Peterson, & Williams, 1998; McFarland, Miller, & Neale, 1990; Njoku, 1995; Njoku & Li, 1999; Weng & Grody, 1998) and for land surface wetness studies (Basist et al., 1998; Giddings & Choudhury, 1989; Paloscia, Macelloni, Santi, & Koike, 2001; Prigent, Matthews, Aires, & Rossow, 2001; Zhang & Armstrong, 2001). Our objective here is to describe a new, very simple yet still efficient algorithm to derive the surface temperature and the fraction of water surface over snow-free areas in sub-arctic and mid-latitude areas from microwave brightness temperatures using an observed linear relationship between horizontal and vertical emissivities at 19 and 37 GHz. The results are compared to independent measurements from different sources: surface water coverage maps, in situ air and ground temperatures, and satellite thermal infrared (IR) temperatures.

2. Microwave data and processing

More than 20 years of spaceborne microwave radiometer observations of the Earth's surface are now available from the Nimbus 7-Scanning Multichannel Microwave Radiometer (SMMR), which operated from 1979 to 1987, and the Defense Meteorological Satellite Program-Special Sensor Microwave/Imager (SSM/I), from 1987 up to now (Maslanik & Stroeve, 2000). These data, NOAA/NASA Pathfinder SSM/I Level 3 EASE-Grid brightness temperatures, were obtained from the EOSDIS National Snow and Ice Data Center (NSIDC) Distributed Active Archive Center, University of Colorado at Boulder, USA. Brightness temperatures consist of gridded data in a Northern Hemisphere Equal Area Scalable Earth-Grid (EASE-Grid) projection. They are provided at a 25-km resolution and, at a given location in our study area, up to two measurements per day are available (ascending and descending pass).

The SMMR and SSM/I instruments provide measurements of the energy emitted by the Earth's surface at several frequencies and at both vertical (V) and horizontal (H) polarizations (Table 1). The SMMR operated at 6.6, 10.7, 18, 21, and 37 GHz. The SSM/I operated at 19.35, 22.2, 37, and 85.5 GHz. Our study is restricted to the 19 (18) and 37 GHz frequencies because they are available on both sensors (SMMR and SSM/I) and they are less affected by atmospheric effects than the 21 or 85 GHz channels.

2.1. Vertical–horizontal emissivity relationship and water effect

Global maps of emissivities over continental areas were obtained by Prigent, Rossow, and Matthews (1997, 1998) from SSM/I measurements, assuming that the thermal IR surface temperature corresponds to the microwave emission effective temperature. International Satellite Cloud Climatology Project (ISCCP) data were used to select cloud-free pixels, thermal IR satellite measurements were used for surface temperatures and the National Center for Environmental Prediction (NCEP) meteorological reanalysis was used for the atmospheric parameters. The spatial resolution of the emissivity database is 30 km. From these data, a significant linear relationship is found between vertical and horizontal emissivities at 19 and 37 GHz. An example is given in Fig. 1 for a large continental area over North America, lying between 45N–70N and 60W–170W, for the month of July 1987. The equations of the regression lines, which fit to the 14064 data are:

$$\text{at 19 GHz: } e_{19V} = 0.562 \times e_{19H} + 0.434 \quad (1a)$$

$$\text{at 37 GHz: } e_{37V} = 0.502 \times e_{37H} + 0.484 \quad (1b)$$

where $e_{19V(H)}$ and $e_{37V(H)}$ are the emissivities at 19 and 37 GHz, horizontal (H) or vertical (V) polarization. Similar equations were found using August data over the same area. The same analysis was also carried out for a large part of northern Russia lying between 50N–70N and 30E–90E. The corresponding equations, based on 8682 data, are very similar:

$$e_{19V} = 0.566 \times e_{19H} + 0.429$$

$$e_{37V} = 0.513 \times e_{37H} + 0.472$$

These relationships are also similar to Mätzler (1994), who found $e_V = 0.46 \times e_H + 0.52$ from ground measure-

Table 1
Frequency (polarization), size of the footprints and operating period for the SMMR and SSM/I channels used

Sensor	SMMR		SSM/I	
Frequency (GHz)	18 (H,V)	37 (H,V)	19.35 (H,V)	37 (H,V)
Footprint size (km)	55 × 41	27 × 18	70 × 45	38 × 30
Operating period	1979–1987		1987–on going	

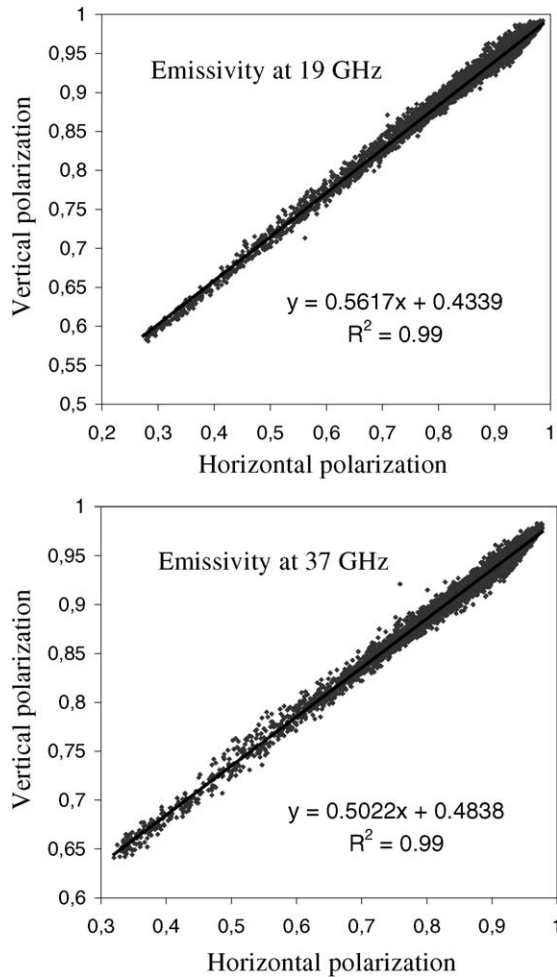


Fig. 1. Emissivity at vertical polarization versus emissivity at horizontal polarization, for the month of July 1987, for an area lying between 45N–70N and 60W–170W over North America (14064 data). The data are from Prigent et al. (1997).

ments at 10.4 GHz in the Alps over snow-free winter land surfaces and to Goïta and Royer (2002), who found $e_{19V} = 0.560 \times e_{19H} + 0.428$ and $e_{37V} = 0.597 \times e_{37H} + 0.401$ using satellite data over northern Quebec in Canada.

From the emissivity data set over Canada, linear relationships are also found between emissivities at 19 and 37 GHz:

$$\text{at vertical polarization: } e_{19V} = 1.212 \times e_{37V} - 0.195$$

$$\text{at horizontal polarization: } e_{19H} = 1.087 \times e_{37H} - 0.079$$

We consider that the variation of emissivities, from 0.3 to 0.99 at 19 GHz horizontal polarization, for example, is mainly due to the presence of water in the pixel. This is also the main hypothesis of Basist et al. (1998) when computing surface temperatures from microwave data.

Microwave emissivities are strongly affected by the percentage of water bodies in the observed pixel even in vegetated areas (Giddings & Choudhury, 1989; Sippel, Hamilton, Melack, & Novo, 1998) because the water emissivity is quite smaller than for most other Earth surfaces (Prigent et al., 1997). They also are affected by the soil moisture in the first few centimeters (Owe et al., 1999; Vinnikov et al., 1999) and by the vegetation (Prigent, Aires, Rossow, & Matthews, 2001) but to a lesser extent. For example, using the HUT microwave emission model (Helsinki University of Technology, Pulliainen, Grandell, & Hallikainen, 1999) it was found that, at 37 GHz, a variation of 30% of open water induces a relative emissivity difference of 10% at vertical polarization (18% at horizontal polarization), while a variation of 30% of the soil volumetric water content induces a relative emissivity difference of 3% at vertical polarization (4% at horizontal polarization). Indeed, the lowest end-points of the data clusters in Fig. 1 correspond well to the open water emissivities (ew), obtained from the Fresnel equations, at an incidence angle of 53.1° and assuming pure water dielectric constant at 10°C (Ulaby, Moore, & Fung, 1986, Eqs. (E14) to (E19)):

$$\text{at 19 GHz: } ew_{19H} = 0.27 \text{ and } ew_{19V} = 0.59$$

$$\text{at 37 GHz: } ew_{37H} = 0.33 \text{ and } ew_{37V} = 0.66$$

Since only liquid water emissivities are considered, the relation is no longer valid if the water bodies are frozen. We also assume that the surface temperature is similar for all the frequencies and polarizations. This is only true if the penetration depth is small. It is not valid over very dry desert areas (Prigent, Rossow, Matthews, & Marticorena, 1999) and over snow-covered areas because the penetration depth of electromagnetic waves in dry snow is very different at 19 and 37 GHz (Surdyk, 2002). Indeed, if winter data are used instead of July data, as in Fig. 1, there is a lot more scatter and no simple relationship is found between both emissivities. In the following, Eqs. (1a) and (1b) are used to derive physical surface parameters from the measured signal at satellite level.

2.2. Land surface temperature and fraction of water surface determination

At a given polarization p , for any frequency, the apparent brightness temperature TB_p at satellite level can be written:

$$TB_p = ep \times t \times Ts + (1 - ep) \times t \times Tad + Tau \quad (2)$$

With ep : emissivity at polarization p ; t : atmospheric transmission; Tad : downward atmospheric contribution; Tau :

upward atmospheric contribution; T_s : land surface temperature. If $eV = a \times eH + b$, as shown in Fig. 1 Eqs. (1a) and (1b), the surface temperature is:

$$T_s = (TBV - a \times TBH - (1 - b - a) \times t \times T_{ad} - \tau_{at} \times (1 - a)) / (t \times b) \quad (3)$$

We can then derive two sets of temperatures (T_{s19} and T_{s37}), one for each frequency. From this temperature (Eq. (3)), the emissivity can be computed as:

$$e_p = (TB_p - t \times \tau_{at} - T_{ad}) / (t \times (T_s - T_{ad})) \quad (4)$$

and finally, the Fraction of Water Surface (FWS) in the observed pixel can be estimated as:

$$FWS = (e_p - e_{dry}) / (e_w - e_{dry}) \quad (5)$$

where e_{dry} is the emissivity of a dry surface and e_w is the emissivity of water.

The fraction of water surface (FWS) which is derived from microwave measurements corresponds to the combination of different contributions (Basist et al., 1998; Prigent, Matthews, et al., 2001) including surface-water bodies,

saturated wet lands, swamps, marshes, or fens, all types of wetlands that are very abundant in sub-arctic areas (Fig. 2). It is also related to the soil moisture in the first few centimeters. The emissivity decreases when the soil moisture increases (Owe et al., 1999) and when the percentage of water bodies in the pixel increases. Even if the later effect is significantly higher than the first one (Njoku & Li, 1999; Prigent, Aires, et al., 2001), it is not possible to discriminate those two components from passive microwave brightness temperatures only.

In order to analyze long-term microwave brightness temperature series, we prefer to use the data without any additional information on atmospheric conditions because it is incomplete for the 24 years of microwave measurements. ISCCP cloud cover is available since 1983 but not cloud water content. Meteorological analyses (NCEP or ECMWF) are also available, but they are very model dependent where not many meteorological data are available as in Arctic areas. Therefore, we apply only a simple unique atmospheric correction at each frequency. The atmospheric transmission (t) and the atmospheric temperature components (τ_{at} and T_{ad}) are estimated from the atmospheric module of the HUT snow emission model (Pulliainen et al., 1999), assuming no clouds and a mean constant integrated water vapour content of 1.5 g/cm^2 which is realistic for summer

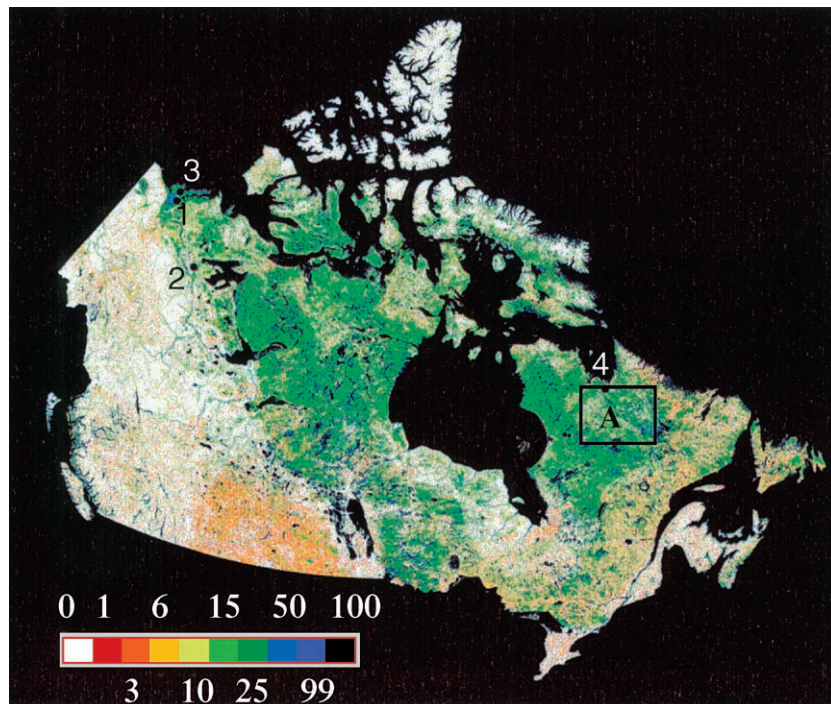


Fig. 2. Fraction of water surface (FWS) of Canada (1 km^2 grid cells). Water covered areas are defined as all waterbody entities (lakes, wetlands, fens, etc.) reported in the Canadian National Topographic Database. Colors correspond from red to blue respectively to 1%, 3%, 6%, 10%, 15%, 25%, 50% and 99% water fraction per pixel, White corresponds to 0% and black to 100% (lakes). Meteorological stations: (1) Inuvik (68.3°N , 226.5°W); (2) Norman Wells (65.2°N , 233.5°W); (3) Parsons Lake (69°N , 226.4°W); (4) Kuujuaq (58.10°N , 68.42°W). The rectangle [A] corresponds to the AVHRR-NOAA images used for the validation analysis over the Province of Quebec. This image was produced by the Canada Centre for Remote Sensing, Natural Resources Canada, Ottawa, Ontario, Canada.

sub-arctic and mid-latitude atmospheres (Bokoye et al., 2001). This gives:

at 19 GHz: $t = 0.919$, $\tau = 21.5$ K, $T_{ad} = 24.0$ K

at 37 GHz: $t = 0.888$, $\tau = 29.3$ K, $T_{ad} = 31.8$ K

The sensitivity of the results to atmospheric parameters is discussed further.

3. Results

3.1. Fraction of water surface

In order to validate our assumptions, we first compare the percentage of water in a pixel computed with microwave data to the water fraction coverage database of Canada, available from the Canada Centre for Remote Sensing (Natural Resources Canada, Ottawa, Ontario, Canada), which gives the fraction (percentage) of surface water coverage for each 1×1 km pixel where information is available (Fig. 2). The product was derived by aggregating vector maps surveyed by the Center for Topographic Information of Natural Resources Canada over the last 30 years.

The surveys are from a combination of air photo and satellite mapping but are rigorously checked for positional accuracy at the time of survey. The majority of the National Topographic Database source maps were surveyed within the growing season (post snow-melt) and should therefore be relatively unbiased during this season in the absence of drought or severe precipitation events (Fernandes, Pavlic, Chen, & Fraser, 2001).

From this database, the FWS values are aggregated at the 25×25 km pixel resolution on the EASE-Grid geographical projection (Fig. 3a). When no information is available, the pixel is assumed to contain 0% water, and therefore the map could underestimate the FWS, mainly in dry areas.

Fig. 3b shows the mean percentage of water (FWS) computed from Eq. (5), using all the July 2000 SSM/I data at 37 GHz. The emissivity is computed at vertical polarization (Eq. (4)) and $\epsilon_{dry} = 0.97$. The 0.97 value, corresponding approximately to the upper end-point of the scatter plot in Fig. 1b, was chosen to give the best correspondence between the two maps (CCRS and SSM/I derived). It certainly depends on the type of land cover and could be more precisely defined in more specific studies. Basist et al. (1998) used 0.95 instead of 0.97 for dry surfaces. This 0.02 emissivity difference would give a relative difference of about 3% on the final water percentage result. The two maps, microwave-derived and CCRS, are very similar, which confirms that the fraction of surface water is the main parameter controlling the emissivity variation at the 25-km resolution in these areas. The results

obtained at 19 GHz (with $\epsilon_{dry} = 0.99$, not shown) are very similar. The main differences between the CCRS and the microwave-derived maps are found along the border and the coasts due to registration and resolution problems; it must be remembered that the original resolution of the microwave measurement is larger than 25 km (Table 1). Large differences are also found over the islands in the Arctic ocean where our method is no longer valid due to the presence of snow and glaciers. The root mean square difference between the two FWS maps over a large Canadian continental land mass zone without coastal and border areas (4782 pixels) is about 6% at both frequencies. The mean difference is less than 1.5% with 70% of the difference values lower than 5%. Similar results were obtained with brightness temperatures from a different year or from August instead of July data. The mean monthly interannual FWS variations are of the order of a few percents.

Fig. 4b illustrates the daily variation in water fractions at a given site (Parsons Lake site, see Fig. 2 and Table 2) which results from seasonal (weather-induced) fluctuations in surface water extent and soil moisture content. These fluctuations appear significant from 15% to 20% after the spring snow-melt period (between days 150 and 170) to 25–35% during the summer period (days 190–270, year 1999) (Fig. 4b). Such a FWS variation induces a large decrease of up to 20 K in brightness temperature at horizontal polarization (Fig. 4a). The FWS high-frequency variations at Parsons Lake are also due to the fact that the sensor footprint varies according to the satellite orbit. From the July 2000 microwave-derived map at 37 GHz, the FWS varies from 21% to 38% in the 3×3 pixels area around Parsons Lake. From the CCRS map, it varies from 9% to 56%. The microwave-derived map is smoothed because the size of the footprint is larger than 25 km.

3.2. Microwave-derived surface temperatures

From Eq. (3), two different land surface temperatures can be obtained from microwave brightness temperatures at 19 and 37 GHz measurements. They are differently affected by atmospheric effects—clouds and water vapour mainly—as well as by changes in surface emissivity due to different surface conditions. The results are compared with ground “in situ” temperatures and satellite IR-derived temperatures. In order to eliminate the points that do not satisfy the preliminary hypothesis (no snow, no frozen water), as well as erroneous data, we simply assume that the emissivities computed at 19 and 37 GHz must also fit the relationship obtained between them from the emissivity database (Prigent et al., 1997) as already seen:

$$\text{abs}(e_{19V} - 1.212 e_{37V} + 0.195)$$

$$< 0.025 \text{ with abs} = \text{absolute value}$$

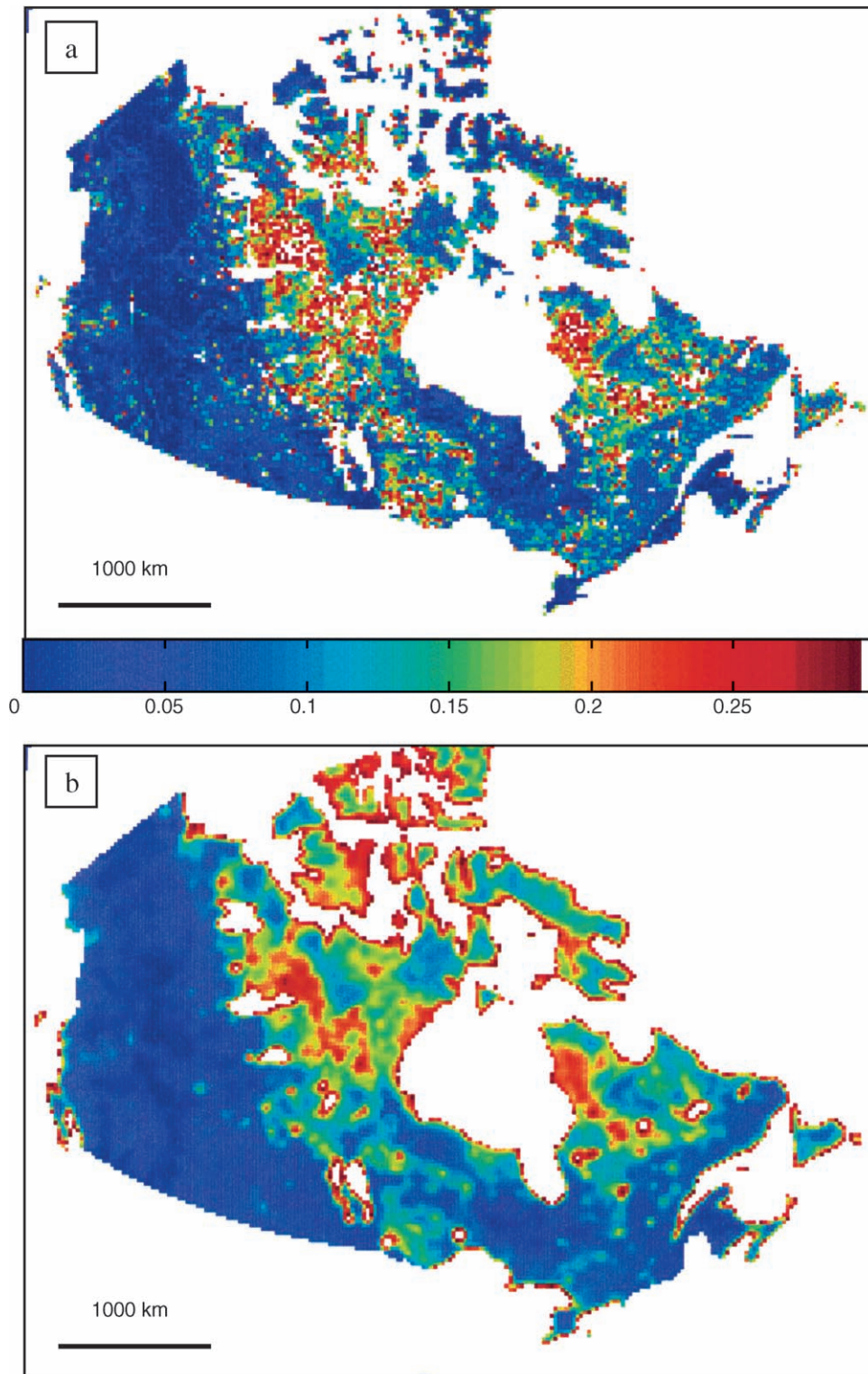


Fig. 3. (a) Surface water coverage (%) of Canada, provided by CCRS, averaged at the 25 km resolution on the EASE-Grid projection (b) Surface water coverage (%) obtained from July 2000 SSM/I data at 37 GHz.

3.3. Comparison with ground temperatures

The microwave-derived surface temperatures are now compared to ground-based land surface and air temper-

atures. The first measurements were provided by C. Tarnocai of Agriculture and Agri-Food Canada. They are ground temperatures at 2.5-cm depth at Parsons Lake (68.97N, 226.45W) in the Mackenzie delta (Northwest territories,

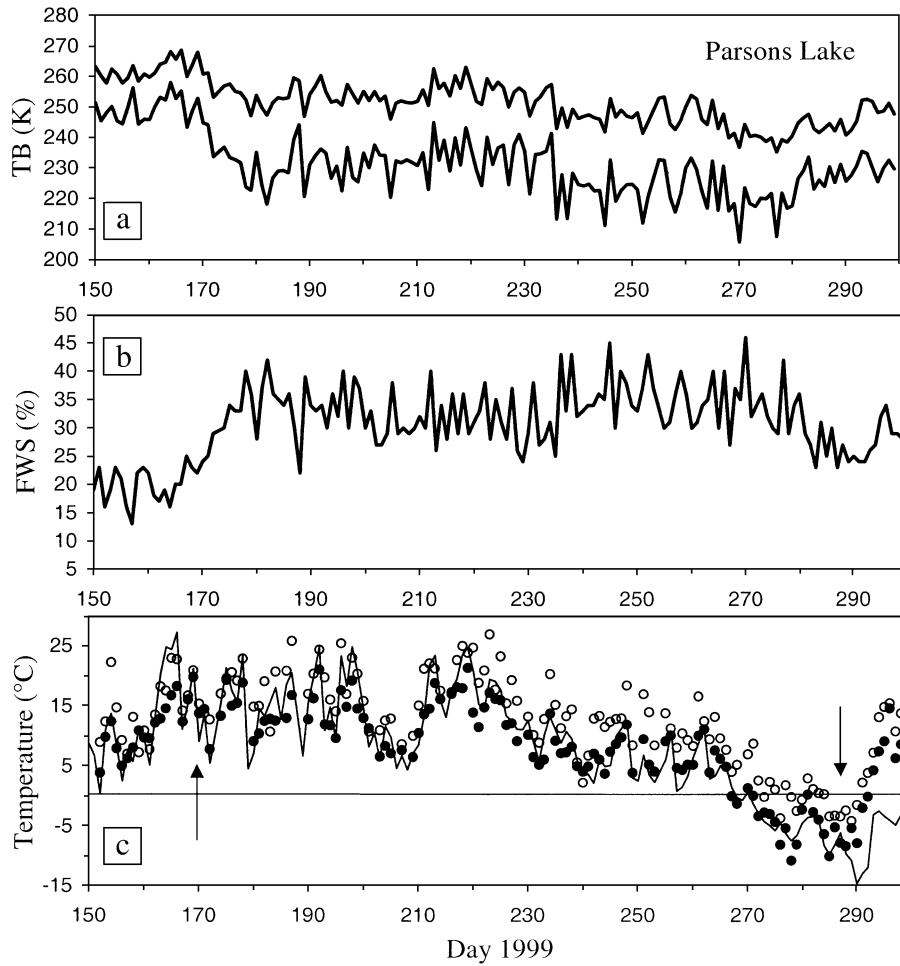


Fig. 4. Parsons Lake, summer 1999, ascending pass data: (a) SSM/I brightness temperatures at 37 GHz. The upper curve is at vertical polarization and the lower one at horizontal polarization. (b) Fraction of Water Surface (FWS) derived from SSM/I brightness temperatures at 37 GHz. (c) Ground (2.5-cm depth) and SSM/I derived temperatures at 19 GHz (open circles) and 37 GHz (black dots). The arrows show the time of the beginning and the end of the snow free season determined from a ratio between the brightness temperatures at 19 and 37 GHz.

Canada) close to the Arctic ocean (Fig. 2), one measurement every 6 h for the years 1999 and 2000. The vegetation is low shrubby tundra (Tarnocai, 2002). The in situ ground meas-

urements are interpolated in order to be synchronous with the satellite overpasses, i.e. 1 h GMT or 18 h Canadian Mountain Time, the day before, for ascending pass, and 16 h

Table 2
Temperature differences between ground based measurements and satellite derived data for different sites and for the two SSM/I frequencies (19 and 37 GHz)

Site and data	FWS(SSM/I)	Orbit period	r.m.s difference (K)		Mean difference (K)		Number of data
			19 GHz	37 GHz	19 GHz	37 GHz	
Norman Wells 65.2 N–233.53 W air temperature, hourly	10–15 %	Ascending Summer 1996	3.2	2.3	–2.0	–0.9	85
		Descending Summer 1996	4.6	2.8	–3.9	–2.0	82
Inuvik 68.3 N–226.52 W air temperature, hourly	15–35 %	Ascending Summer 1996	4.2	2.5	–0.6	0.2	83
		Descending Summer 1996	3.3	3.1	0.3	–1.9	80
Parsons Lake 68.97 N–226.45 W	15–40%	Ascending Summer 1999	5.05	2.7	3.9	–0.8	107
		Descending Summer 1999	5.7	2.5	–4.7	–1.5	112
Ground (–2.5 cm) interpolated temperature from 6-hourly data	15–40%	Ascending Summer 2000	4.5	4.1	2.4	–2.6	94
		Descending Summer 2000	4.2	2.1	–2.8	0.1	101
AVHRR Image Northern Quebec	5–25%	May–June 1991	3.9	2.7	–3.0	–1.2	31

The average fraction of water surface (FWS) is computed from the SSM/I data corresponding to the same pixel and the same period of time. Local time at Normal Wells, Inuvik and Parsons Lake is about 18 h for ascending pass and 9 h for descending pass.

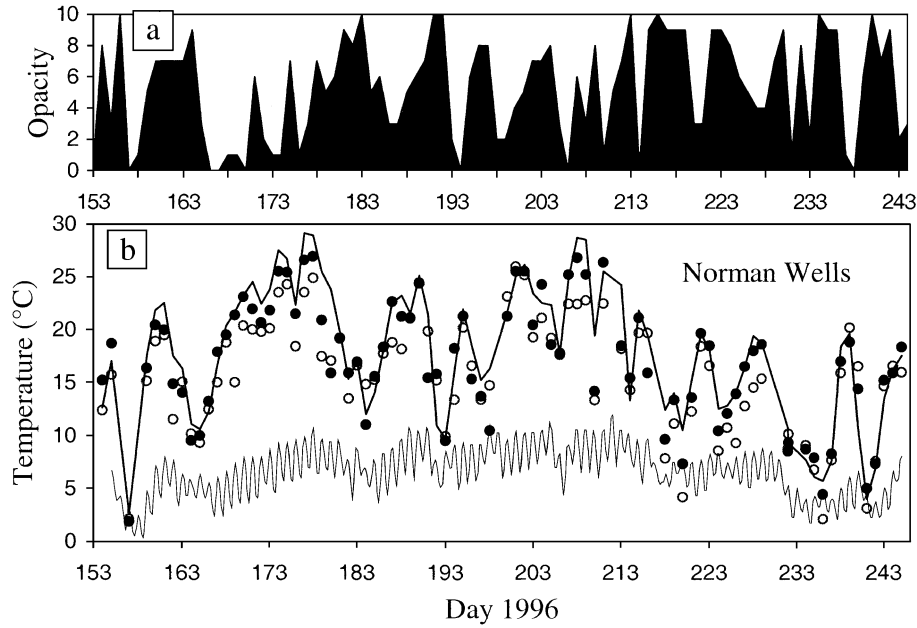


Fig. 5. Norman Wells, summer 1996, ascending pass data: (a) Cloud opacity, in tenths, at the same time as ascending pass measurements. (b) Surface air (thick line), ground (5-cm depth, thin line) and SSM/I derived temperatures at 19 GHz (open circles) and 37 GHz (black dots).

GMT or 9 h Mountain Time the same day for descending pass. It is found that, most of the time, the microwave-derived temperatures are close to the in situ measured surface temperatures (Fig. 4c, Table 2) despite the fact no cloud screening is applied and in spite of a very rapidly changing spectral signature (Fig. 4a). One must consider also that only one measurement is available every 6 h and that the interpolation might induce errors of several degrees. Differences are also expected between the in situ data and the microwave-derived temperatures because the percentage of water in the pixel is high and the thermal inertia of water is larger than the soil's. High-ground temperature peaks are therefore smoothed by nearby cold water; this is particularly true for the 19 GHz channel and also explains differences between ascending and descending pass results because the sensor footprints are not exactly the same and contain a different fraction of water. Otherwise, large differences occur at the beginning and at the end of summer when

snow or ice is still present in the observed pixel (Fig. 4c). In particular, positive temperatures may be found above land when lakes are still ice covered at the beginning of summer. From a simple algorithm based on the ratio of the brightness temperatures at 19 and 37 GHz (Hallikainen & Jolma, 1992; Walker & Goodison, 1993), snow- and ice-contaminated pixels are detected independently. The beginning and the end of the snow-free period as defined by this algorithm are shown (arrows) in Fig. 4c. They correspond, especially at the end of summer, to the time when the deduced temperature is very different from the in situ data. The r.m.s. differences between ground temperatures and microwave-derived temperatures are computed only for the snow-free period, they are about 4–5 K at 19 GHz and 2–4 K at 37 GHz (Table 2). The increase in wetness around day 170 (17 June) corresponds to a decrease in the brightness temperature but to an increase in the polarization difference and the land surface temperature. This behavior clearly prohibits the

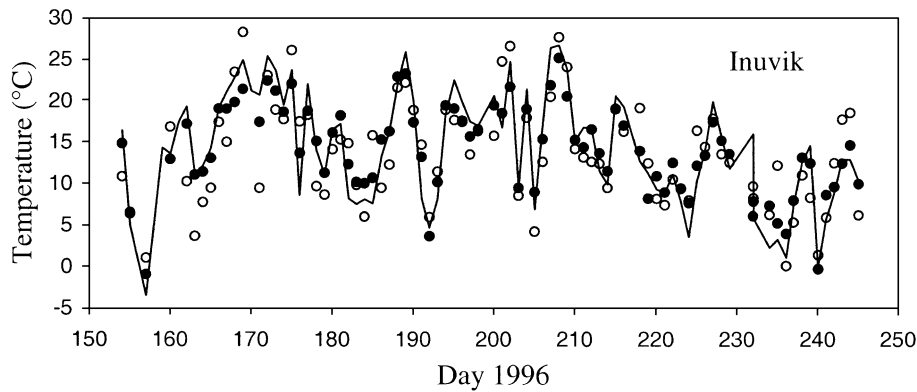


Fig. 6. Inuvik, summer 1996, ascending pass data. Surface air (line) and SSM/I derived temperatures at 19 GHz (open circles) and 37 GHz (black dots).

use of a single mean emissivity for surface temperature determination.

A second example is from another site located in the Mackenzie valley at Norman Wells (65.2N–233.53W). Ground temperatures, every hour, at -5 cm were provided by M. Nixon of the Geological Survey of Canada for the year 1996. Surface air temperatures were also available from a nearby meteorological station. These temperatures are compared to the microwave-derived temperatures at the same time ± 1 h (Fig. 5b). The site is located in the boreal forest (Fig. 2) and a large difference is found between the air temperature and the ground temperature. The microwave-derived temperatures are close to the air temperature reflecting better the forest temperature seen by the radiometer: the r.m.s. difference is between 2 and 5 K (Table 2). As to Parsons Lake, better results are obtained with the 37 GHz channel. Cloud opacity was available from the nearby meteorological station. The data corresponding to the time of ascending pass are given in Fig. 5a and are very similar for the descending pass. The cloud cover is very dense most of the time and does not significantly affect the microwave signal but would prohibit the use of satellite IR measurements.

The same conclusions arose from the comparison of our results with the surface air temperatures measured at the Inuvik meteorological station (68.3N–226.52W, Table 2, Fig. 6) in spite of a very different fraction of water surface in the SSM/I pixel: about 10–15% at Norman Wells and 15–35% at Inuvik. There are less variations in the fraction of water surface at Norman Wells because the site is more homogeneous (Fig. 2) and a slightly different footprint does not really change the type of surface coverage.

3.4. Comparison with satellite IR-derived temperatures

Surface temperatures derived from NOAA-10/AVHRR IR measurements, at the same scale as coincident SSM/I brightness temperatures, are used for validation as a completely independent data set (Goïta & Royer, 2002). The first advantage of this data set is that the same surface is taken into account by both methods (IR and microwave) instead of comparing an in situ spot measurement with a large footprint microwave data. The second advantage of this data set is that the NOAA/AVHRR data at 1-km resolution were also used to carefully select pixels without cloud and large water bodies. The areas extracted from the satellite images cover the taiga and tundra regions in northern Quebec (Fig. 2) in May (9) and June (16–17) 1991. The acquisition times of SSM/I and NOAA-10 are the same within 30 min, so that they can be accurately compared.

Both AVHRR and SSM/I images were first geometrically registered and projected in the same projection with a spatial resolution of 1 and 25 km, respectively (one SSM/I pixel includes 625 AVHRR pixels). Original SSM/I swath data were provided by A. Walker from the Meteorological

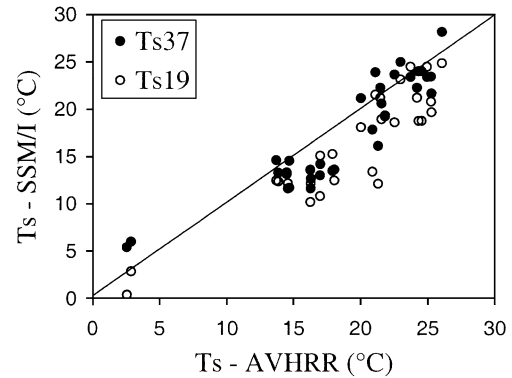


Fig. 7. Microwave-derived surface temperatures at 19 GHz (open circles) and 37 GHz (black dots) versus NOAA/AVHRR thermal IR derived temperature over sub-arctic areas in Quebec in May and June 1991.

Service of Canada. AVHRR data were corrected for atmospheric effects using radiosoundings and the MODTRAN software. A constant IR emissivity value of 0.97 was considered for channel 4, following Goïta, Royer, and Bussi eres (1997). Water bodies and cloudy pixels were carefully removed from the analysis using thresholds on visible, near infrared and thermal radiances. The stringent constraint imposed with respect to cloudiness at the 1-km resolution limits the number of selected pixels. The IR-derived final temperature is the mean of all the temperatures corresponding to the 625 AVHRR pixels.

The SSM/I-derived temperatures, using the same methodology as previously described (Eqs. (1a), (1b), and (3)) are compared to AVHRR-derived temperatures in Fig. 7. Several pixels from the first image (May 9) were eliminated by applying the same simple algorithm based on the ratio of the brightness temperatures at 19 and 37 GHz. Meteorological records confirm that these pixels were snow contaminated. The overall comparison is good, showing better results than obtained previously with the 37 GHz channel (mean bias of -1.0 K, Table 2).

4. Discussion

The proposed surface parameter determination algorithm is very simple and depends only on a few parameters: a and b coefficients (Eqs. (1a) and (1b)) and atmospheric transmission and emission (Eq. (2)). The a and b coefficients are determined from measurements over North America using SSM/I data and are coherent with physically based estimates. They mainly depend on the fraction of water surface, which is the dominant factor, and also on the type of land coverage as well as on the type of sensor used due to calibration differences. Since the algorithm is based on the difference between the two polarizations, which can be small, the retrieval algorithm is highly sensitive to the value of these coefficients. A variation of 1% of a or b , taken independently, would induce a difference of about 5 K on

the derived temperature. However, in practice, they vary in opposite ways (see, for example, the previous comparison between Canadian and Russian relationships) and the effect of their variations tends to balance this sensitivity (see Eq. (3)). Nevertheless, an accurate determination of a and b is necessary and this work is supported by a very strong and stable emissivity relationship derived from the emissivity data set obtained by Prigent et al. (1997). In other areas where water effect is small, the type of land coverage should be taken into account (Prigent, Matthews, et al., 2001). We compared the summer values for both FWS and temperatures for the same areas and several years and the coherency of the observed variations shows the robustness of our method.

It is very promising that the results are relatively insensitive to cloud coverage (Fig. 5) and that constant atmospheric parameters can be taken without large errors. For a given area (such as Northern latitudes), it is possible to apply our methodology to the analysis of 24 years of satellite microwave brightness temperatures without ancillary data to specify the atmospheric parameters. The sensitivity of the microwave-derived temperature is about 3–4 K for a variation of 1% of the atmospheric transmission and the results are almost directly linked to the upward atmospheric contribution but these two parameters vary in opposite ways. A second calculation was carried out for the Inuvik data (year 1996, ascending + descending pass) with a very different integrated water vapour content: 0 instead of 1.5 g/cm². In this case, the atmospheric transmission varies from 0.928 to 0.888 at 37 GHz and from 0.980 to 0.919 at 19 GHz, and the upward atmospheric contributions vary from 18 to 29 K at 37 GHz and from 5 to 21 K at 19 GHz. Despite these large differences, the mean microwave-derived temperature varies only from 11.22 to 11.19 °C at 37 GHz and from 11.39 to 12.17 °C at 19 GHz. This is due to the fact that our method is mainly based on the polarization difference which is insensitive to atmospheric water vapour. However, for a global analysis, better results would be obtained if realistic atmospheric parameters from ancillary data were used. Further tests must be carried out to determine the required accuracy in atmospheric parameters to significantly increase the accuracy of the derived land surface temperature.

Better results are obtained at 37 GHz in spite of the larger sensitivity of this channel to clouds compared to the 19 GHz channel. It could be explained by the fact that 19 GHz emissivity is more dependent on surface conditions such as wetness and on the larger size of the footprint at 19 GHz (Table 1), which renders comparison with ground data more difficult. Lastly, our approach based on the polarized emissivity relationship (Eqs. (1a) and (1b)) is only valid for land surfaces free of snow, lake ice, and frozen ground. This hypothesis can be efficiently satisfied by applying systematically a simple algorithm, based on the brightness temperatures, which eliminates contaminated pixels (Grody & Basist, 1996; Walker & Goodison, 1993).

5. Conclusion

A linear relationship is found between microwave (19 and 37 GHz) surface emissivities at horizontal and vertical polarizations over snow- and ice-free areas. Assuming that the effective microwave temperature is unique, it is then possible to retrieve surface emissivity and surface temperature from microwave brightness temperatures obtained by satellite sensors after atmospheric corrections.

Over the Canadian sub-arctic continental area, it is found that the fraction of water surface within a pixel is the main factor modifying emissivity. Global maps of fraction of water surface are obtained which are similar to an independent map within a few percents. The microwave-derived surface temperatures are compared to synchronous in situ air and ground surface temperatures and also with independent satellite IR measurements over areas without snow or ice. The average root mean squared difference is $2.8 \pm 0.6^\circ$ for all the analyzed sites using the 37-GHz channel. Better results are always obtained with the 37-GHz channel compared to the 19 GHz channel. When there is dense vegetation, the microwave-derived temperature is closer to the surface air temperature than to the ground temperature. The quality of the results is not sensitive to cloud cover.

The methodology is particularly well adapted to sub-arctic areas where the fraction of surface water is important and quite variable. The fact that surface temperatures are obtainable, even when the sky is cloudy, is a main advantage compared to thermal IR-based measurements. It will be used to study temperature trends and fraction of water surface variations from the available 24 years of satellite microwave data.

Acknowledgements

The study was funded by the French ACI Observation de la Terre, Le Centre Jacques Cartier, NSERC, Canada, and the CRYSYS project, Meteorological Service of Canada. The in situ temperature data were kindly provided by C. Tarnocai, Agriculture and Agri-Food Canada, and M. Nixon, Geological Survey of Canada. This work was carried out when M. Fily was at CARTEL, Université de Sherbrooke, on leave from LGGE, Grenoble.

References

- Aires, F., Prigent, C., Rossow, W. B., & Rothstein, M. (2001). A neural network approach including first-guess for retrieval of atmospheric water vapor, cloud liquid water path, surface temperature and emissivities over land from satellite microwave observations. *J. Geophys. Res.*, *106*, 14887–14907.
- Basist, A., Grody, N. C., Peterson, T. C., & Williams, C. N. (1998). Using the Special Sensor Microwave/Imager to monitor land surface temperatures, wetness, and snow cover. *J. Appl. Meteorol.*, *37*, 888–911.
- Bokoye, A. I., Royer, A., O'Neill, N. T., Fedosejevs, G., Teillet, P. M.,

- McArthur, L. J. B., & Cliche, P. (2001). Characterization of atmospheric aerosols across Canada from a ground-based sunphotometer network: AEROCAN. *Atmos.-Ocean*, 39(4), 429–456.
- Burgess, M., Smith, S., Brown, J., & Romanovsky, V. (2001). The Global Terrestrial Network for Permafrost (GTN-P), Status Report. Submitted to the IPA Executive Committee Meeting, Rome. Available online: <http://sts.gsc.nrcan.gc.ca/gtnp/index.html>.
- Cavaliere, D. J., Gloersen, P., Parkinson, C. L., Comiso, J. C., & Zwally, H. J. (1997). Observed hemispheric asymmetry in global sea ice changes. *Science*, 278, 1104–1106.
- Chang, A. T. C., Foster, J. L., & Hall, D. K. (1987). Nimbus-7 SSMR derived global snow cover parameters. *Ann. Glaciol.*, 9, 39–44.
- CLIC (2001). Climate and Cryosphere project. In I. Allison, R.G. Barry & B. Goodison, *Science and co-ordination plan*, WRCP-114, WMO/TD 1053.
- Fernandes, R. A., Pavlic, G., Chen, W., & Fraser, R. (2001). Canada wide 1-km water fraction derived from National Topographic Data Base maps. *Nat. Resour. Canada*. <http://geogratis.cgdi.gc.ca/download/waterFraction>.
- Giddings, L., & Choudhury, B. J. (1989). Observation of hydrological feature with Nimbus-7 37 GHz data applied to South America. *Int. J. Remote Sens.*, 10, 1673–1686.
- Goïta, K., & Royer, A. (2002). Combination of passive microwave and thermal infrared for the retrieval and analysis of microwave emissivities and temperature. *IGARSS 2002, Toronto, June*.
- Goïta, K., Royer, A., & Bussi eres, N. (1997). Characterization of land surface thermal structure from NOAA-AVHRR data over a northern ecosystem. *Remote Sens. Environ.*, 60, 282–298.
- Grody, N. C., & Basist, A. N. (1996). Global identification of snowcover using SSM/I measurements. *IEEE Trans. Geosci. Remote Sens.*, 34, 237–249.
- Hallikainen, M. T., & Jolma, P. A. (1992). Comparison of algorithms for retrieval of snow water equivalent from Nimbus-7 SMMR data in Finland. *IEEE Trans. Geosci. Remote Sens.*, 30(1), 124–131.
- McFarland, M. J., Miller, R. N., & Neale, C. M. U. (1990). Land surface temperature derived from the SSM/I passive microwave brightness temperatures. *IEEE Trans. Geosci. Remote Sens.*, 28, 839–845.
- Maslanik, J., & Stroeve, J. (2000). 1990–March 2000. DMSP SSM/I daily polar gridded brightness temperatures. *CD-ROM, NSIDC*. Colorado, USA: University of Boulder.
- M atzler, C. (1994). Passive microwave signatures of landscapes in winter. *Meteorol. Atmos. Phys.*, 54, 241–260.
- Njoku, E. G. (1995). Surface temperature estimation over land using satellite microwave radiometry. In B. J. Choudhury, Y. H. Kerr, E. G. Njoku, & P. Pampaloni (Eds.), *Passive microwave remote sensing of land atmosphere interactions* (pp. 509–530). Utrecht, The Netherlands: VSP.
- Njoku, E. G., & Li, L. (1999). Retrieval of land surface parameters using passive microwave measurements at 6–18 GHz. *IEEE Trans. Geosci. Remote Sens.*, 37, 79–93.
- Owe, M., Van de Griend, A. A., de Jeu, R., de Vries, J. J., Seyhan, E., & Engman, E. T. (1999). Estimating soil moisture from satellite microwave observations: past and ongoing projects, and relevance to GCIP. *J. Geophys. Res.*, 104, 19735–19742.
- Paloscia, S., Macelloni, G., Santi, E., & Koike, T. (2001). A multifrequency algorithm for the retrieval of soil moisture on a large scale using microwave data from SMMR and SSM/I satellites. *IEEE Trans. Geosci. Remote Sens.*, 39, 1655–1661.
- Prigent, C., Aires, F., Rossow, W. B., & Matthews, E. (2001). Joint characterization of vegetation by satellite observations from visible to microwave wavelength: a sensitivity analysis. *J. Geophys. Res.*, 106, 20665–20685.
- Prigent, C., Matthews, E., Aires, F., & Rossow, W. B. (2001). Remote sensing of global wetland dynamics with multiple satellite data sets. *Geophys. Res. Lett.*, 28, 4631–4634.
- Prigent, C., Rossow, W. B., & Matthews, E. (1997). Microwave land surface emissivities estimated from SSM/I observations. *J. Geophys. Res.*, 102(D18), 21867–21890.
- Prigent, C., Rossow, W. B., & Matthews, E. (1998). Global maps of microwave land surface emissivities: potential for land surface characterization. *Radio Sci.*, 33, 745–751.
- Prigent, C., Rossow, W. B., Matthews, E., & Marticorena, B. (1999). Microwave radiometric signatures of different surface types in deserts. *J. Geophys. Res.*, 104(D10), 12147–12158.
- Pulliainen, J., Grandell, T., & Hallikainen, J. (1999). Hut snow emission model and its applicability to snow water equivalent retrieval. *IEEE Trans. Geosci. Remote Sens.*, 37, 1378–1390.
- Serreze, M. C., Walsh, J. R., Chapin III, F. S., Osterkamp, T., Dyurgerov, M., Romanovsky, V., Oechel, W. D., Morison, J., Zhang, T., & Barry, G. (2000). Observational evidence of recent change in the northern high-latitude environment. *Clim. Change*, 46, 159–207.
- Sippel, S. J., Hamilton, S. K., Melack, J. M., & Novo, E. M. M. (1998). Passive microwave observations of inundation area and area/stage relation in the Amazon River floodplain. *Int. J. Remote Sens.*, 19, 3055–3074.
- Smith, S. L., & Burgess, M. M. (1998). Mapping the response of permafrost in Canada to climate warming. *Current Research, Geological Survey of Canada, 1998-E*, 163–171.
- Smith, S. L., Burgess, M. M., & Heginbottom, J. A. (2001). Permafrost in Canada, a challenge to northern development. In G. R. Brooks (Ed.), *A synthesis of geological hazards in Canada. Geological Survey of Canada Bulletin, vol. 548* (pp. 241–264). Ottawa: Natural resources.
- Surdyk, S. (2002). Using microwave brightness temperature to detect short-term surface air temperature changes in Antarctica: an analytical approach. *Remote Sens. Environ.*, 80(2), 256–271.
- Tamocai, C. (2002). *Agriculture and agri-food Canada*. Personal Communication.
- Torinesi, O., Fily, M., & Genthon, C. (2003). Interannual variability and trend of the Antarctic summer melting period from 20 years of spaceborne microwave data. *J. Climate* (in press).
- Ulaby, F. T., Moore, R. K., & Fung, A. K. (1986). *Microwave remote sensing, active and passive, vol. 3*. Dedham, MA, USA: Artech House.
- Vinnikov, K. Y., Robock, A., Qiu, A. S., Entin, J. K., Owe, M., Choudhury, B. J., Hollinger, S. E., & Njoku, E. G. (1999). Satellite remote sensing of soil moisture in Illinois, United States. *J. Geophys. Res.*, 104, 4145–4168.
- Walker, A. E., & Goodison, B. E. (1993). Discrimination of a wet snow cover using passive microwave satellite data. *Ann. Glaciol.*, 17, 307–311.
- Weng, F., & Grody, N. C. (1998). Physical retrieval of land surface temperature using the spectral sensor microwave imager. *J. Geophys. Res.*, 103(D8), 8839–8848.
- Zhang, T., & Armstrong, R. L. (2001). Soil freeze/thaw cycles over snow-free land detected by passive microwave remote sensing. *Geophys. Res. Lett.*, 28(5), 763–766.